AGU PUBLICATIONS

JGR

Journal of Geophysical Research: Atmospheres

RESEARCH ARTICLE

10.1002/2014JD022458

Key Points:
- UFP collection efficiency (ϵ) for four broadleaf species was measured
- Rougher surfaces enhance ϵ even for hydraulically smooth flow
- Longer leaf dimension has a thicker quasi-laminar boundary layer and smaller ϵ

Correspondence to:
M. Y. Lin,
m_lin@mail.ncku.edu.tw

Citation:
Huang, C. W., M. Y. Lin, A. Khlystov, and G. G. Katul (2015), The effects of leaf size and microroughness on the branch-scale collection efficiency of ultrafine particles, *J. Geophys. Res. Atmos.*, *120*, doi:10.1002/2014JD022458.

Received 19 AUG 2014
Accepted 5 FEB 2015
Accepted article online 2 MAR 2015

The effects of leaf size and microroughness on the branch-scale collection efficiency of ultrafine particles

C. W. Huang[1], M. Y. Lin[2], A. Khlystov[3], and G. G. Katul[1,4]

[1]Nicholas School of the Environment, Duke University, Durham, North Carolina, USA, [2]Department of Environmental and Occupational Health, College of Medicine, National Cheng Kung University, Tainan, Taiwan, [3]Division of Atmospheric Sciences, Desert Research Institute, Reno, Nevada, USA, [4]Department of Civil and Environmental Engineering, Duke University, Durham, North Carolina, USA

Abstract Wind tunnel experiments were performed to explore how leaf size and leaf microroughness impact the collection efficiency of ultrafine particles (UFP) at the branch scale. A porous media model previously used to characterize UFP deposition onto conifers (*Pinus taeda* and *Juniperus chinensis*) was employed to interpret these wind tunnel measurements for four different broadleaf species (*Ilex cornuta*, *Quercus alba*, *Magnolia grandiflora*, and *Lonicera fragrantissima*) and three wind speed (0.3–0.9 m s^{-1}) conditions. Among the four broadleaf species considered, *Ilex cornuta* with its partially folded shape and sharp edges was the most efficient at collecting UFP followed by the other three flat-shaped broadleaf species. The findings here suggest that a connection must exist between UFP collection and leaf dimension and roughness. This connection is shown to be primarily due to the thickness of a quasi-laminar boundary layer pinned to the leaf surface assuming the flow over a leaf resembles that of a flat plate. A scaling analysis that utilizes a three-sublayer depositional model for a flat plate of finite size and roughness embedded within the quasi-laminar boundary layer illustrates these connections. The analysis shows that a longer leaf dimension allows for thicker quasi-laminar boundary layers to develop. A thicker quasi-laminar boundary layer depth in turn increases the overall resistance to UFP deposition due to an increase in the diffusional path length thereby reducing the leaf-scale UFP collection efficiency. It is suggested that the effects of leaf microroughness are less relevant to the UFP collection efficiency than are the leaf dimensions for the four broadleaf species explored here.

1. Introduction

While the significance of ultrafine particles (UFP, particles with diameter smaller than 100 nm) is rarely questioned in climate, air quality, and human health sciences [*Oberdörster*, 2001; *Oberdörster et al.*, 2005; *Peters et al.*, 1997], the pathways by which UFP sources and sinks impact their concentration continue to draw significant research attention. The sources of UFP are attributed to anthropogenic origins (e.g., factory emissions and diesel exhaust from cars [*Holmn and Ayala*, 2002]) and natural sources such as biomass burning and gas to particle conversion in the biosphere [*Altshuller*, 1985; *Buzea et al.*, 2007; *McMurry and Wilson*, 1982; *Pryor et al.*, 2008a; *Seinfeld and Pandis*, 2006; *Zimmerman et al.*, 1978]. One of the main sinks for UFP over land is the expansive vegetation cover, though fluxes of UFP may be occasionally bidirectional [*Pryor et al.*, 2008a, 2008b]. Given the large areal extent of vegetated surfaces [*Sexton et al.*, 2013], their contribution to the overall UFP sink is known to be of primary importance [*Andreae and Crutzen*, 1997]. Due to the small size of UFP, the collection mechanism by vegetation is dominated by Brownian diffusion. The relation between the vegetation collection term (S_{cv}), the leaf-level laminar boundary layer conductance (g_a), the local turbulent friction velocity (u_τ), and the Schmidt number (S_c) is described by parameters that are presumed to arise from interaction between the flow adjacent to the leaf and leaf properties. It is precisely the connections between such parameters, UFP removal efficiency by vegetation, and leaf properties that have resisted complete treatment and frame the scope of this work. The relation between S_{cv}, g_a, u_τ, and S_c is used in virtually all operational UFP deposition models, whether they be big leaf schemes [*Wesely and Hicks*, 2000] in climate models, rough boundary layers used in air quality models [*Feng*, 2008], or multilayered models used in ecosystem studies [*Huang et al.*, 2014; *Katul et al.*, 2010; *Petroff et al.*, 2008a, 2008b]. Specifically, when g_a is expressed as $u_\tau \theta S_c^{-\gamma}$, the two empirical parameters θ and γ encoding the

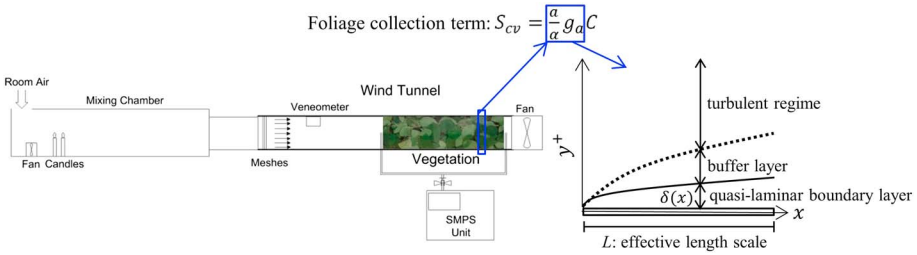

Figure 1. Schematic showing the wind tunnel setup and how the particle deposition processes within the vegetated medium are interpreted as a "flat" plate at the leaf level. Note that δ is the thickness of the quasi-laminar boundary layer and y^+ is the dimensionless distance from the surface (see discussions in section 4.3 and Appendix A), which is defined as $y^+ = yu_v/\nu$, where u_v is the friction velocity governed by skin friction and ν is the kinematic viscosity.

interaction between the flow and leaf morphology must be a priori specified. It was suggested elsewhere [*Seinfeld and Pandis*, 2006; *Zhang et al.*, 2001] that a $\theta = 3$ and a γ that varies from 1/2 to 2/3 depending on surface roughness (surrogated to land-cover type) be employed in operational models for UFP removal. However, major differences between measured and modeled UFP sinks [*Pryor et al.*, 2009] have already been noted above tall forested sites when such representation is employed (by factors ranging from 3 to 5). This discrepancy may be partly attributed to uncertainty in how foliage attributes impact θ and γ. In fact, recent wind tunnel experiments [*Huang et al.*, 2013] reported θ to vary with leaf attributes consistent with earlier work [*Slinn*, 1982] and γ to vary with particle size groups.

Motivated by a possible dependency of θ and γ on leaf attributes and particle size, wind tunnel experiments were conducted here on the collection efficiency of UFP for four different broadleaf species and then compared to similar experiments on coniferous species. The UFP concentration measurements were interpreted using a recently proposed porous media model that can be inverted to infer the relation between S_{cv}, g_a, and S_c across various wind speeds for each of the broadleaf species considered. The porous media model used here was recently shown to be consistent with previous theories (e.g., *Lin et al.* [2014]) such as filtration theory that treats vegetation as fibrous filters [*Davidson et al.*, 1982; *Lin and Khlystov*, 2012]. Also, this model was previously employed to characterize UFP deposition onto conifers such as Pine and Juniper [*Huang et al.*, 2013; *Lin et al.*, 2012], thereby allowing direct comparisons between the findings from the wind tunnel experiments here and previous findings on coniferous species. Furthermore, the g_a deduced from the experiments here is then linked to leaf size and microroughness using a deposition model that utilizes a prototypical mean velocity and total (molecular and turbulent) viscosity profiles above smooth flat plates [*Browne*, 1974; *Davies*, 1966; *Hussein et al.*, 2012; *Lai and Nazaroff*, 2000; *Piskunov*, 2009; *Wood*, 1981; *Zhao and Wu*, 2006a, 2006b]. The goal of this model development is to assist in disentangling how leaf size and microroughness impact θ and γ separately and hence the UFP collection efficiency.

2. Experiment

In the wind tunnel experiment shown in Figure 1, four broadleaf species (Table 1 and Figure 2) representing different leaf sizes were selected: *Ilex cornuta* (Needleholly), *Quercus alba* (Oak), *Magnolia grandiflora*

Table 1. Summary of the Vegetation Attributes in the Present (Broadleaf Species) and Previous (Coniferous) Wind Tunnel Studies

Species	LAI ($m^2\ m^{-2}$)	Packing Density (PD) ($m^3\ m^{-3}$)	Shape	Length[a]
Ilex cornuta	213	0.063	Partially folded	~5 cm
Quercus alba	237	0.033	Flat	~15 cm
Magnolia grandiflora	210	0.058	Flat	~30 cm
Lonicera fragrantissima	250	0.066	Flat	~5 cm
Juniperus chinesis[b]	222	0.117	Needlelike	~2 mm

[a]Note that the length of the four broadleaf species and Juniper are the average longest length of leaves and the average diameter, respectively.
[b]Similar wind tunnel setup using Juniper branches by *Huang et al.* [2013].

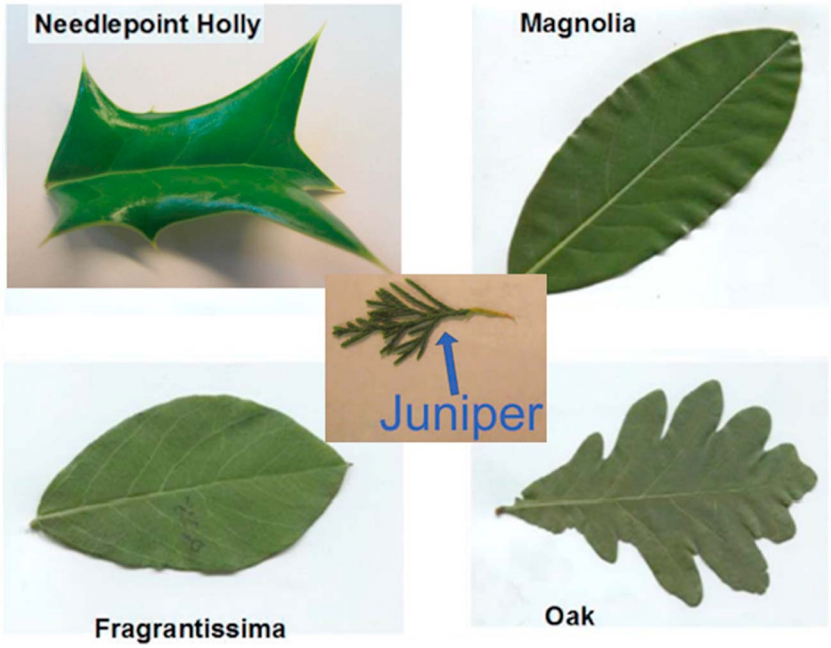

Figure 2. Morphology of the four broadleaf species and the coniferous species from previous study [*Huang et al.*, 2013], i.e., *Ilex cornuta* (Needleholly), *Quercus alba* (Oak), *Magnolia grandiflora* (Magnolia), *Lonicera fragrantissima* (Fragrantissima), and *Juniperus chinensis* (Juniper).

(Magnolia), and *Lonicera fragrantissima* (Fragrantissima). The total (two-sided) leaf area index (LAI) (i.e., total surface area of the exposed foliage available for deposition) in the present wind tunnel experiments was arranged to be similar (i.e., 210–250 $m^2\ m^{-2}$) to that of earlier studies using *Juniperus chinensis* branches [*Huang et al.*, 2013] so that differences in UFP collection between coniferous and broadleaf species can be further assessed. Description of the wind tunnel setup can be found elsewhere [*Huang et al.*, 2013]. However, for completeness, salient features of the experiment are repeated. The UFP were generated by burning candles in a large mixing chamber (30 cm wide, 57 cm high, and 545 cm in length). A fan positioned inside the mixing chamber was then used to facilitate the mixing of the generated UFP with room air. The particle number concentration of unfiltered room air, in which the maximum and minimum particle number concentration was ±30% of $5 \times 10^3\ cm^{-3}$ in the mixing chamber, roughly remained constant and negligible compared with the generated particle concentration from burning candles (approximately $5.5 \times 10^4\ cm^{-3}$). The air from the mixing chamber was then drawn into the wind tunnel (16 cm wide, 18 cm high, and 226 cm in length) through an aluminum tube (385 cm long and 18 cm in diameter) at a constant flow rate. The charge of the UFP entering the wind tunnel was close to equilibrium [*Buckley et al.*, 2008] thereby eliminating the need for a neutralizer. Three plastic mesh screens were placed near the inlet of the wind tunnel to ensure that the turbulence was well developed and the UFP mix is homogenized. A vanometer (model 480 Dwyer) was placed between the meshes and the broadleaf species to record the time and cross-sectional area-averaged wind speed (U_o) upwind of the vegetated section. A digital thermometer and barometer (Cole-Parmer YO-90080â02) was also placed at the end of the wind tunnel section to measure room air temperature (T) and atmospheric pressure (P). The vegetated section contained branches uniformly placed near the exit of the wind tunnel across a length $L_x = 0.84$ m. A Scanning Mobility Particle Sizer (SMPS, model 3080 TSI) used for obtaining size distribution scans (measured size range is from 12.6 nm to 102 nm) was connected to the two sampling ports located at the beginning and the end of the test section. Prior to every experiment, UFP loss through the two sampling ports was separately measured in the absence of vegetation. The particle loss did not exceed 10% and was accounted for when calculating the UFP vegetation collection efficiency. For each of the four broadleaf species, particle collection efficiency was measured for $U_o = 0.3$, 0.6, and 0.9 $m\ s^{-1}$. For each configuration (i.e., each combination of species type and U_o), seven tests were made. Each test contained one upstream and one downstream size distribution scan (each scan time was 120 s consisting of 90 s upscan and 30 s downscan). A dual-port digital manometer (model 621 TPI) with two silicon tubes was used to measure the static pressure drop across the vegetated

section (= L_x). At the end of the experiment, the broadleaf leaves within the vegetated section were placed in a scanner (Epson Perfection V30), and Adobe Photoshop CS6 was employed to convert image pixels into leaf area. The total foliage volume within the test section was determined by submerging the branches and leaves in water contained in a 1 L graduated cylinder (SIBATA). The broadleaf foliage volume was then divided by the volume of the test section (0.84 m long by 0.3 m wide by 0.57 m high) to determine the packing density (PD). The foliage characteristics are summarized in Table 1.

3. Interpreting the Wind Tunnel Experiments Using a Porous Media Model

To infer the relation between S_{cv}, g_a, and S_c across various U_o and for all four broadleaf species, a porous media model that upscales from leaf to branch level is used. Details about the model formulation and assumptions can be found elsewhere [*Huang et al.*, 2013]. Briefly, this model is based on a size-resolved mean particle continuity equation that describes the horizontal air movement along L_x and is given by

$$U\frac{\partial C(x)}{\partial x} = -\frac{\partial F_c(x)}{\partial x} - S_{cv}(x), \tag{1}$$

where x is the downstream distance with $x = 0$ just upstream of the vegetated section, $U \approx U_0/(1 - \mathrm{PD})$ is the time and area-averaged velocity within the vegetated section assumed to be independent of x by virtue of the constant flow rate used in the experiments, $C(x)$ is the UFP mean concentration for particles with diameter d_p, $S_{cv}(x)$ is the UFP collection dominated by Brownian diffusion, and $F_c(x) \approx -(D_m + D_t)\partial C(x)/\partial x$ is the combined molecular and turbulent flux with the latter closed using a gradient-diffusion scheme, $D_m = (k_B T/3\pi\mu d_p)C_c$ is the particle molecular diffusivity (independent of x), k_B is the Boltzmann constant, T is the absolute temperature, μ is the dynamic air viscosity, $C_c = 1 + (\lambda_a/d_p)(2.514 + 0.8\exp(-0.55 d_p/\lambda_a))$ is the Cunningham coefficient, λ_a is the mean free path between air molecules, and $D_t = K_t(1 + \tau_p/\tau)^{-1}$ is the particle turbulent diffusivity related to the turbulent viscosity K_t. The turbulent viscosity is given by $K_t = u_\tau l_m$ [*Prandtl*, 1925], where $u_\tau = \sqrt{\tau_o/\rho}$ is a local turbulent friction velocity formed by both skin friction and form drag, τ_o is the total stress, ρ is the mean air density, and l_m is the effective mixing length (described later). For UFP, $\tau_p/\tau \ll 1$ resulting in $D_t \approx K_t$ [*Katul et al.*, 2010], where τ_p and τ are the particle and turbulent relaxation time scales, respectively. Inside dense vegetated medium, the more restrictive mixing length on momentum transport is given by $l_m = 2\beta^3 L_c$, where the momentum absorption $\beta = 0.3$ [*Finnigan and Belcher*, 2004; *Poggi et al.*, 2004; *Raupach*, 1994] and $L_c = (C_d a)^{-1} \approx |\partial P/\partial x|/(\rho U^2)$ is the adjustment length scale, a is the total (two-sided) leaf area density approximated as LAI/L_x for uniformly distributed vegetation, P is the mean pressure, and C_d is a bulk drag coefficient (including both viscous c_v and form c_f drag) that can be inferred from the pressure gradient using

$$C_d \approx \frac{1}{a}[|\partial P/\partial x|/(\rho U^2)] \approx \frac{1}{a}\frac{\Delta P}{L_x}\frac{1}{\rho U^2}, \tag{2}$$

where ΔP is the measured pressure drop over L_x. For a constant mean wind velocity inside the vegetated area, the friction velocity can be determined from $u_\tau = \sqrt{C_d U^2}$, which is based on the velocity-squared law used to describe the local momentum transfer. Hence, from measured $\partial P/\partial x$, $a = \mathrm{LAI}/L_x$, PD, and U_o, C_d can be determined, followed by u_τ, l_m, and K_t as described above. Moreover, the UFP concentration at leaf surfaces is assumed to be much smaller than the ambient concentration within the vegetated section for all d_p so that the collection term S_{cv} reduces to

$$S_{cv} = \frac{a}{\alpha} g_a C, \tag{3}$$

where g_a is, as before, the laminar boundary layer conductance on the leaf assuming that Brownian diffusion dominates the UFP collection mechanism [*Huang et al.*, 2013] and α is a shape factor adjusting the projected area to the total leaf surface area of leaves. Hence, $\alpha = \pi$ for needlelike leaves [*Huang et al.*, 2013, 2014; *Katul et al.*, 2010, 2011; *Lin et al.*, 2012] and $\alpha = 1$ for broadleaf species when LAI is defined as two sided. As noted in section 1, g_a in operational models for the vegetated medium is given as [*Slinn*, 1982]

$$g_a = u_\tau \left(\theta S_c^{-\gamma}\right), \tag{4}$$

where $Sc = \nu/D_m$ is the molecular Schmidt number, ν is the kinematic viscosity (=μ/ρ), and γ and θ are the two sought-after model parameters (discussed later) in this wind tunnel experiment to be related to leaf attributes, microroughness, or particle size group [*Huang et al.*, 2013].

After substituting the above parameters into equation (1) and defining the normalized concentration as $\hat{C}(x) = C(x)/C(0)$ and downstream distance as $\hat{x} = x/L_x$, the normalized mean continuity equation (1) becomes

$$\frac{\partial^2 \hat{C}}{\partial \hat{x}^2} - P_1 \frac{\partial \hat{C}}{\partial \hat{x}} - D_2 = 0, \tag{5}$$

where $P_1 = UL_x/(D_m + D_t)$ and $D_2 = (\mathrm{LAI})g_a L_x/(D_m + D_t)$ are the Peclet and type 2 Damkohler numbers, respectively. Solving equation (5) requires the specification of two boundary conditions selected here as $\hat{C}(0) = 1$ and $\partial \hat{C}/\partial \hat{x}|_{\hat{x}=1} = 0$. For broadleaf species (i.e., π is excluded) with uniformly distributed a within the test section, the analytical solution is given by

$$\frac{C(x)}{C(0)} = \hat{C}(x) = \frac{\exp\left(\frac{P_1}{2}\hat{x}\right)\left[\lambda \cosh\left(\frac{\lambda}{2}\left(\hat{x}-1\right)\right) - P_1 \sinh\left(\frac{\lambda}{2}\left(\hat{x}-1\right)\right)\right]}{\lambda \cosh\left(\frac{\lambda}{2}\right) - P_1 \sinh\left(\frac{\lambda}{2}\right)}, \tag{6}$$

where $\lambda = \sqrt{4D_2 + P_1^2}$. The normalized concentration at the end of the vegetated section, $\hat{C}(1)$, is equivalent to the so-called penetration ratio (Pe). It can be analytically determined from equation (6) by setting $\hat{x} = 1$ to yield

$$Pe = \frac{\exp\left(\frac{P_1}{2}\right)}{\cosh\left(\frac{\lambda}{2}\right) + \frac{P_1}{\lambda}\sinh\left(\frac{\lambda}{2}\right)}. \tag{7}$$

Also, Pe can be related to the UFP collection efficiency ($= \epsilon$) using $Pe = 1 - \epsilon$.

4. Results and Discussions

Since the flow properties L_c, l_m, K_t, and eventually Pe and ϵ require C_d, the estimated C_d for each U_o is first presented for the four broadleaf vegetation types. Next, the effective θ and γ are determined so that differences between measured and modeled Pe are minimized for all four species. Finally, the connection between θ and γ as well as leaf attributes (i.e., size and microroughness) are discussed, thereby completing the study objectives.

4.1. Branch-Scale Aerodynamic Properties

A major advantage of the wind tunnel setup here is that C_d can be estimated from U_o, a, and dP/dx thereby enabling the computation of turbulent aerodynamic properties (i.e., u_τ and K_t) and subsequently the key parameters related to the particle collection (i.e., g_a and S_{cv}) assumed to be spatially uniform within the vegetated section. Because of this spatial uniformity in turbulent aerodynamic properties, the UFP deposition can be interpreted as if g_a and S_{cv} apply to an effective leaf dimension representing the aggregate of all leaves comprising a within the test section. How C_d varies with U_o for the four broadleaf species is first discussed. As shown in Figure 3, while the measured C_d for the three species (i.e., Needleholly, Oak, and Fragrantissima) decreases with increasing bulk Reynolds number (i.e., $Re = UL_x/\nu$) and tends to reach a constant at higher Re (i.e., $U_o \geq 0.6\ \mathrm{m\ s^{-1}}$), C_d for the Magnolia case appears to be invariant to the Re variations here. The choice of L_x in the representation of Re is rather subjective but is selected here as an external length scale over which the pressure drop driving the flow occurs. Other length scales such as the adjustment length scale or the effective size of eddies responsible for momentum transport may be even more appropriate (i.e., L_c or l_m instead of L_x). However, the estimation of such length scales requires C_d, which then leads to (artificial) self-correlation between C_d and Re when such length scales are employed in the Reynolds number definition. It is for this reason that Re is presented based on L_x instead of local length scales appropriate to momentum transfer. Based on the $Re = UL_x/\nu$, the reduction trend in C_d with increasing Re may be attributed to several factors including the so-called "sheltering effect" induced by neighboring foliage elements, possible realignments of leaves at higher wind speeds adjusting the frontal shape and main leaf dimension exposed to the bulk flow, and viscous effects [*Brunet et al.*, 1994; *Finnigan*, 2000; *Raupach and Thom*, 1981; *Thom*, 1968]. These reductions have been noted in a few previous wind tunnel studies in which coniferous as well as broadleaf species were used [*Cao et al.*, 2012; *Huang et al.*, 2013]. The C_d values for the broadleaf species are compared with coniferous species (i.e., Juniper) having similar LAI reported elsewhere [*Huang et al.*, 2013]. The comparison indicates that the C_d for Juniper falls

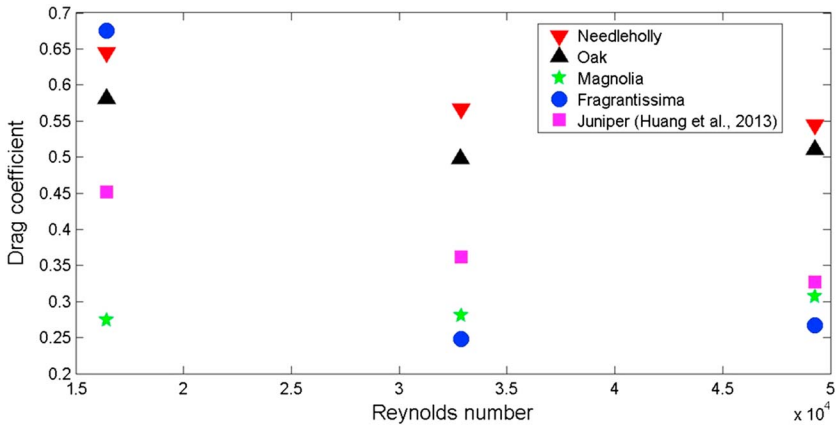

Figure 3. The computed drag coefficient (C_d) at different bulk Reynolds number ($Re = UL_x/\nu$) for the four broadleaf and coniferous species. The previous experiments on Juniper are also added for reference.

within the range of these four broadleaf species. It is to be noted that the C_d reduction for Juniper can be attributed to sheltering effects due to its high PD. The high PD leaves no space for realignments [*Huang et al.*, 2013] (see Table 1). For the three broadleaf species here (i.e., Needleholly, Oak, and Fragrantissima) with small PD values (see Table 1) and soft texture, the effects of realignment along the mean airflow direction at higher U_o (i.e., higher *Re*) may be more significant than sheltering effects resulting in reduced C_d [*Molina-Aiz et al.*, 2006]. For Magnolia, however, the nearly constant C_d (around 0.28) at different *Re* can be attributed to the small sheltering effects due to its low PD and firm texture resisting any realignment. However, differences in sheltering effects, realignments, leaf morphology, and microroughness on leaf surfaces across species cannot be readily distinguished here from C_d given its "bulk" value. Furthermore, the C_d estimated from the pressure drop includes both viscous drag c_v and form drag c_f, and some viscous effects on C_d cannot be entirely excluded.

4.2. Performance of the Porous Media Model for Broadleaf Species

When modeling *Pe*, two empirical parameters associated with the particle collection mechanism for UFP must be a priori specified: θ and γ (discussed later). As suggested elsewhere [*Huang et al.*, 2013], γ may be sensitive to the particle size class (i.e., it may be treated as a constant for UFP), while θ may be dependent on leaf microroughness. As a starting point, γ is taken to be 2/3 (deemed appropriate and justified later for this setup) so as to explore plausible θ values. The performance of the porous media model in reproducing *Pe* for the four broadleaf species is discussed for an optimized θ and $\gamma = 2/3$. As noted elsewhere [*Lin et al.*, 2012], the optimum values of θ for a fixed γ can be determined from a "global search" that minimizes root-mean-square percent error (RMSPE) between modeled and measured *Pe*, which is defined as

$$\mathrm{RMSPE} = \sqrt{\frac{1}{N}\sum_{i=1}^{N}\Delta_i^{\,2}} \times 100, \tag{8}$$

where *N* is the number of data points (i.e., four foliage types across three U_o runs and all particle diameter classes), and Δ_i is the difference between measured and modeled *Pe* computed from equation (7). For $\gamma = 2/3$, optimized θ for the four broadleaf and coniferous species from previous studies [*Huang et al.*, 2013] are listed in Table 2. These optimized θ values are generally smaller for the four broadleaf species here when compared to their coniferous counterparts. Using these optimized θ values and $\gamma = 2/3$ for the UFP collection term, the one-to-one *Pe* comparisons for all runs are shown in Figure 4. This comparison indicates that deviations between modeled and measured *Pe* are within 20% comparable to the measurement error (see also Figure 5) for most data points (~90%). Again, using $\gamma = 2/3$ and the optimized θ values in Table 2, Figure 5 features the agreement between measured and modeled *Pe* across the range of U_o and UFP sizes. The average RMSPE shown here are mostly less than 15%. The UFP collection efficiency as a whole for the broadleaf species appears to be smaller than their coniferous counterparts (i.e., Juniper) with similar $\mathrm{LAI} = \int_0^{L_x} a\,dx$ (see Figure 3 and *Huang et al.* [2013, Figure S1-1]) consistent with previous

Table 2. The Optimized θ Values for a Fixed γ (= 2/3) and an Order of Magnitude Estimation for I_2

Species	θ	$\propto I_2$
Ilex cornuta	0.76	1.2
Quercus alba	0.44	0.96
Magnolia grandiflora	0.51	0.94
Lonicera fragrantissima	0.4	1.08
Juniperus chinesis[a]	0.91	1.59

[a]Similar wind tunnel setup using Juniper branches by *Huang et al.* [2013].

studies [*Beckett et al.*, 2000; *Freer-Smith et al.*, 2004; *Hwang et al.*, 2011; *Zhang et al.*, 2001]. Besides, Needleholly and Magnolia bracket the most and least efficient at collecting UFP among the four broadleaf species (see Figures 4 and 5). A larger UFP collection efficiency appears to be reflected in a larger optimized θ. The analysis here suggests that the porous media model with its parameterization for u_τ, l_m, and D_t can be adequately applied to broadleaf species when the two sought-after parameters θ and γ are appropriately specified. Thus, these two parameters are discussed in the context of leaf morphology (primarily leaf dimension) and microroughness on the leaf surface.

4.3. A Hydraulically Smooth Flat-Plate Analogy

The schematic shown in Figure 1 illustrates the particle deposition process on an isolated flat leaf with dimension L (not connected to L_x or L_c). Particles in ambient air are first transported by turbulence to the vicinity of the leaf surface. These particles must then traverse a quasi-laminar boundary layer (i.e., a disturbed viscous sublayer) pinned to the leaf surface before being deposited on the solid interface [*Seinfeld and Pandis*, 2006]. Finally, particles are collected at the leaf assuming the surface is "clean" (infinite sink) and no rebound occurs (a plausible assumption for UFP). To link these depositional pathways to the leaf dimension and microroughness, a three-sublayer model for the mean velocity and momentum flux is used [*Browne*, 1974; *Davies*, 1966; *Hussein et al.*, 2012; *Lai and Nazaroff*, 2000; *Piskunov*, 2009; *Wood*, 1981; *Zhao and Wu*, 2006a, 2006b]. The three sublayers describing the mean velocity and momentum transport include an outer turbulent region away from the leaf, a transition (or buffer) region, and a viscous region. The choice of three sublayers instead of two (a viscous and a turbulent region) is necessary because the interface between these layers (i.e., buffer region) is dynamic and can shrink or expand depending on the turbulent state and how eddies impinge on the surface. Because the viscous region interfaces this buffer layer that is dynamic and impacted by turbulence, the term quasi-laminar boundary is used throughout. This disturbance induced by eddy impingement from aloft may be sufficiently large to occasionally disturb the laminar state of the viscous region during very short intervals. However, the flow maintains its laminar state in this region on the much longer averaging time period. To avoid complexities associated with leaf geometry and variable angle of attack, the flow immediately above the leaf surface is replaced by a typical boundary layer of thickness δ forming above a flat hydraulically smooth plate of finite dimension. These idealized assumptions are now used to explore the parameterizations of g_a (i.e., θ and γ) in relation to the main leaf dimension L and leaf microroughness. The microroughness elements are first assumed to be characterized by a mean protrusion height k entirely immersed within the viscous region (i.e., $k << \delta$). It is for this reason that the flow is presently labeled as hydraulically smooth. This conceptual framework links the leaf dimension to L, the microroughness of the leaf surface to k, and the thickness of the quasi-laminar boundary layer to δ. In reality (i.e., field conditions), fluctuations in turbulent intensity (low in the wind tunnel experiments here), wind direction (stationary in the wind tunnel experiments here), and wakes originating from neighboring leaves (their spatial

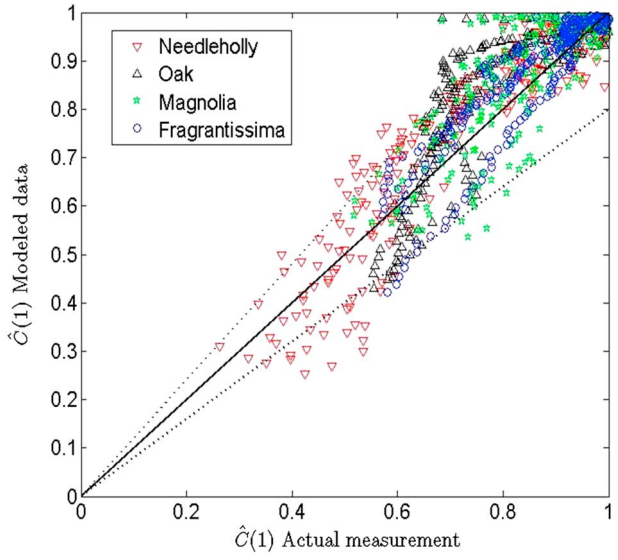

Figure 4. Comparison between measured and modeled penetration for the four broadleaf species and for all particle sizes and wind conditions. The solid line represents 1 : 1 relation, while the dashed line indicates 20% deviation from the solid line.

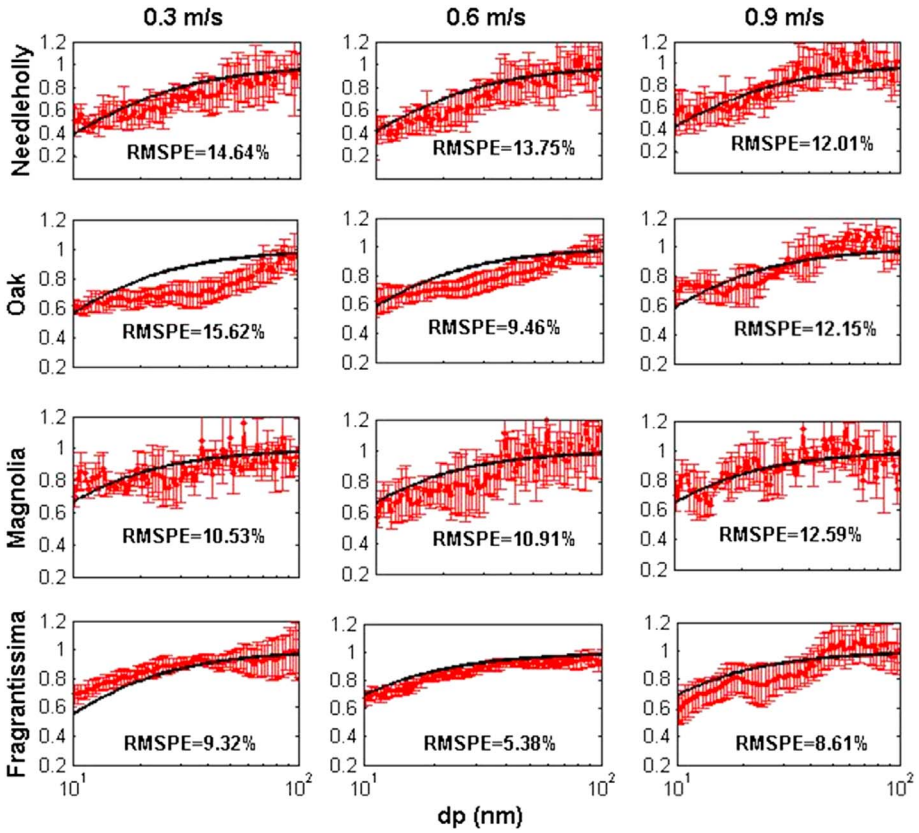

Figure 5. Comparison between measured and modeled penetration (*Pe*) as a function of particle diameter (d_p) at different wind speeds and for all four broadleaf species when using the optimum θ value while setting $\gamma = 2/3$. The error bars in the measurement represent one standard deviation for each particle size comparable to the measurement error (~20%).

extent is quite restricted given the large leaf area in the vegetated section of the wind tunnel considered here) induce large deviations from this conceptual framework. Not withstanding these issues, a primary convenience to such hydraulically smooth flat-plate conceptual framework or analogy is that the mean velocity and eddy viscosity profiles are independent of k. However, particle deposition onto the plate (or leaf surface) may depend on k as discussed later. Details of the three-sublayer model for specifying the mean velocity and eddy diffusivity profiles and particle deposition velocity are presented in Appendix A.

4.3.1. The Effects of Microroughness Height k on γ

Combining the formulations of the quasi-laminar boundary layer conductance for the porous media model and the three-sublayer depositional model (see Appendix B), a dimensionless conductance g_{a_*} spatially averaged over the leaf dimension L can be derived thereby linking θ and γ with leaf size and microroughness. Formulated in this manner, γ can be expressed as a function of d_p and k. To illustrate, assume $T = 300$ K, $P = 101.3$ kPa, and the friction velocity component associated with the viscous drag $u_v = 0.06\ \mathrm{m\ s^{-1}}$. Next, γ as a function of d_p is shown to vary across four different roughness sizes k (i.e., 0, 0.1, 0.7, and 1.1 mm) in Figure 6a. Here the upper limit of k does not exceed the modeled thickness of the quasi-laminar boundary layer (δ) (i.e., the distance between the boundary and the outer edge of the buffer layer; see Appendix A), determined to be approximately at 1.2 mm for hydraulically smooth surfaces for the selected u_v (= $0.06\ \mathrm{m\ s^{-1}}$) here. The selection of u_v is determined by $u_v/u_\tau = (c_v/C_d)^{1/2}$ (see equations (B1) and (B2)), given that $c_v/C_d \approx 1/3$ [*Slinn*, 1982] (though this ratio is expected to depend on leaf attributes and Reynolds number as discussed later) and $u_\tau \approx 0.1\ \mathrm{m\ s^{-1}}$ for dense vegetated medium. The selected u_τ for illustration is smaller than prevalent $u_\tau \approx 0.5\ \mathrm{m\ s^{-1}}$ typical for values "above" forested canopies in natural setting [*Stoy et al.*, 2006] but comparable to typical values of u_τ "within" forested canopies [*Huang et al.*, 2014] and the wind tunnel experiments here. Since $\delta \approx 1.2$ mm is thicker than the leaf body of the four broadleaf species explored here, this may suggest that the assumption of a hydraulically smooth surface is plausible for the wind tunnel experiments here and the coniferous species from a previous study

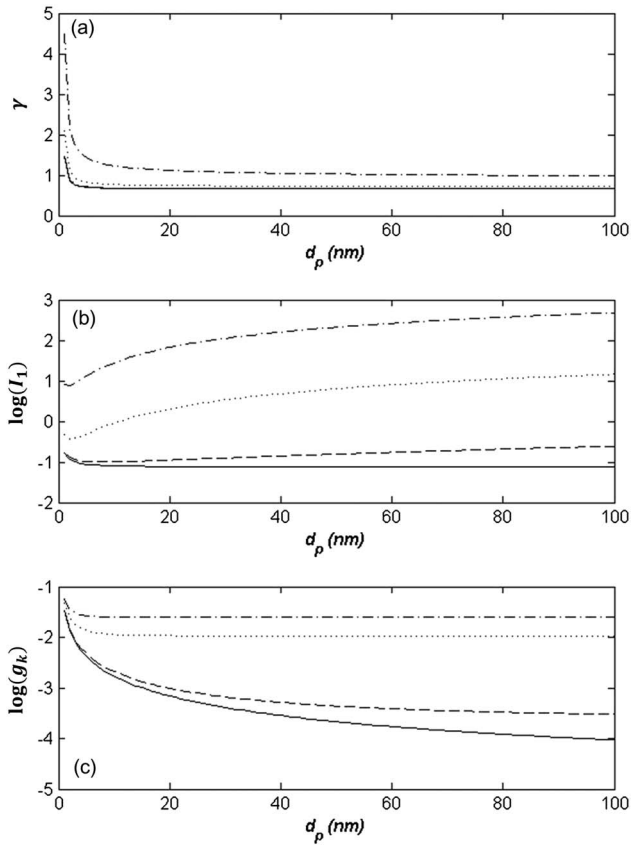

Figure 6. (a) The γ values, (b) the index I_1, and (c) the dimensionless boundary conductance g_k for different heights of microroughness elements k (solid line: 0 mm, dash line: 0.1 mm, dotted line: 0.7 mm, and dash-dotted line: 1.1 mm) as a function of particle diameter (d_p). These results are from the three-layer depositional model for hydraulically smooth plates using $u_v = 0.06\,\mathrm{m\,s^{-1}}$, $T = 300$ K, and $P = 101.3$ kPa.

[*Huang et al.*, 2013]. Stated differently, the k characterizing the microroughness of the leaf surfaces is likely to be smaller than 1.2 mm (i.e., $d_p < k \ll \delta$) (discussed later) even though the exact k values were not measured. If $k \ll \delta$, k is less relevant to the scaling analysis here provided $d_p < k$. From Figure 6a, the following points can be made:

1. For $d_p \leq 10$ nm (i.e., nucleation mode), γ significantly increases from its expected 2/3 value with decreasing d_p and the increasing trend in γ is further enhanced by increasing k.
2. For 10 nm$< d_p \leq 100$ nm (i.e., UFP size range), γ increases with increasing k but can be treated as a constant for a set k . Moreover, γ appears sensitive to k only when $k/\delta > 0.6$ (i.e., $k > 0.7$ mm) and can be as high as $\gamma \approx 1$ for $k \approx \delta$ ($\approx$ 1.2 mm). However, $\gamma \approx 2/3$ when $d_p < k \ll \delta$ as is the case here for the UFP size range and the broadleaf species. This finding provides some justification for the choice of a $\gamma = 2/3$ when comparing the optimized θ values across broadleaf and coniferous species in the aforementioned wind tunnel experiments.

4.3.2. The Effects of Microroughness Height *k* on θ

Based on g_{a_*}, the behavior of θ is now linked to two key variables: the microroughness on the leaf surface and leaf dimension (see equation (B2)). To explore the first effect, an index I_1 (see equation (B3)) can be defined to exclude the effects of leaf dimension on θ. Figure 6b shows the variations in I_1 against d_p for four different k (i.e., 0, 0.1, 0.7, and 1.1 mm). These modeled variations represent how θ may be impacted by k across the UFP size ranges when the leaf size L is held constant. This analysis suggests that θ increases with increasing k for a given d_p. Likewise, θ increases with increasing d_p at a given k. Unlike γ, θ is sensitive to variations in k even when $d_p < k \ll \delta$. From $k = 0$ to 0.1 mm, for example, the average θ value across all d_p increases by a factor of 2. Moreover, θ can be approximately treated as a constant (i.e., $I_1 \approx 0.08$) only for 10 nm $\leq d_p \leq$ 100 nm (i.e., UFP) and only when the leaf surface is completely smooth (i.e., $k = 0$ mm). The above analysis suggests that the choice of a single constant $\theta = 3$ value in all air quality and climate models may not be adequate since no leaf surface is entirely smooth. Furthermore, rougher surfaces whose k is still immersed within the viscous sublayer result in larger θ, which enhances particle deposition velocity even when the flow is hydraulically smooth.

4.3.3. The Effects of Leaf Dimension *L* on θ

Having discussed the effects of leaf microroughness on UFP deposition onto leaf surfaces through the effects of k on θ and γ, the effects of leaf dimension are now discussed. To do so, the established effects of k on θ are excluded and another index I_2 (see equation (B4)) is employed to explore how θ may be impacted by leaf dimension L at a given microroughness k and flow conditions. To show how I_2 can be used to achieve this objective, consider the dependence of θ (i.e., I_2) on c_v/C_d as suggested elsewhere [*Slinn*, 1982] and supported here. The surrogate of θ, I_2, suggests that θ increases with increasing c_v but decreases with increasing C_d. As discussed in section 3, C_d was determined from the wind tunnel experiments here via

pressure drop measurements. On the other hand, c_v for hydraulically smooth surfaces can be linked to the leaf effective length scale L (Figure 1) that allows for the development of the quasi-laminar boundary layer on the leaf surfaces. This value of c_v is given as [*Schlichting*, 1979]

$$c_v = 0.072(Re_l)^{-1/5}, \tag{9}$$

where $Re_l = UL/\nu$ is the leaf-level Reynolds number with the leaf dimension length scale L. The combination of the formulation for θ in equations (B2) and (9) suggests an alternative parameterization for θ when L is known. Equation (9) cannot be prognostically implemented in practice because the precise value of L for a specific species is rarely known and may change with wind direction or foliage realignment as earlier noted. Nevertheless, equation (9) serves a diagnostic purpose. It can be used to assess the importance of leaf dimension on g_a when L is associated with the physical dimension of the leaves along the wind direction. The uniformity of the aerodynamic attributes within the test section (see discussion in section 4.1) and the choice of similar LAI (i.e., a) across all species in the wind tunnel experiments here minimizes any potential interference between a and L, and the discussion of L can be simply based on the physical dimension of leaves. Inserting equation (9) into I_2, I_2 is proportional to $U^{-1/10}L^{-1/10}{C_d}^{-1/2}$, which can be used to examine the differences in θ between broadleaf and coniferous species using the experiments here and the previous wind tunnel experiments on conifers. A number of features are now pointed out:

1. Due to the range of U_o (i.e., 0.3–0.9 m s^{-1}) explored in the wind tunnel experiments here, the small exponent of U (i.e., $-1/10$) in I_2 results in only 10% variation in c_v. This suggests that U does not appreciably impact θ through c_v for the wind tunnel experiments here.
2. The θ values are substantially altered by c_v through L because differences in L across broadleaf and coniferous species are quite large. As shown in Table 1, the expected L for the quasi-laminar boundary layer to grow on the three flat broadleaf species is about 5 cm (for Fragrantissima) to some 30 cm (for Magnolia). For the coniferous leaf, the average diameter of Juniper is only 2 mm and it can be conjectured that L here may be much smaller than 2 mm due to its cylindrical-like shape. Different from the three flat broadleaf species, Needleholly has leaf characteristics in between conifers and its flat-plate hardwood species. The geometry of the Needleholly is partially folded, similar to a semisolid half-folded cylinder, while the other three broadleaf species are mostly flat and more flexible. Moreover, the sharp edge of the Needleholly leaves may generate more wakes and further impede or spatially delay the formation and subsequent growth of the quasi-laminar boundary layer along L. Thus, L for the three flat broadleaf species can be 100 to 1000 times larger than L for Junipers, which is only few times smaller than L for Needleholly. Considering only the effects of L on I_2 (i.e., θ value), this scaling analysis suggests that I_2 for Juniper can be 1.6 to 2 times larger than I_2 for the three flat broadleaf species but slightly larger than I_2 for Needleholly consistent with the experiments here.
3. Ideally, θ must be specified for each d_p as well as U (i.e., C_d in I_2 varies with U), but the optimized θ values listed in Table 2 are computed across all velocities and all particle sizes for each species due to measurement uncertainty (i.e., ~20%). Thus, the optimized θ value can only be discussed in relation to averaged $C_d^{-1/2}$ for each species. The averaged $C_d^{-1/2}$ across all wind velocities for Juniper, Needleholly, Oak, Magnolia, and Fragrantissima are 1.59, 1.31, 1.38, 1.87, and 1.72, respectively. Interestingly, the estimates for I_2 obtained by combining the simultaneous (and counteracting) effects of L and C_d also have similar trends as the optimized θ values (see Table 2). That is, I_2 (or the optimized θ values) for the broadleaf species is generally smaller than those for Juniper given the thinner quasi-laminar boundary layers. Accordingly, a larger UFP collection efficiency can be found (see Figure 5 and *Huang et al.* [2013, Figure S1-1]) for larger I_2 (i.e., a surrogate for θ) associated with L when $d_p < k \ll \delta$ (i.e., $\gamma \approx 2/3$).

4.3.4. The Compensatory Effects of *L* and *k* on θ

As stated before, θ increases with increasing k, while θ is impacted by L in the opposite way. This compensatory effect of k vis-à-vis L on θ (and hence g_a) can be further discussed through another dimensionless conductance g_k (see equation (B5)). The variations in g_k against d_p for four different k (i.e., 0, 0.1, 0.7, and 1.1 mm) under the same condition as before are shown in Figure 6c. It is clear that g_k (i.e., a surrogate for g_a) is larger for smaller d_p only when k is very small (i.e., $k \leq 0.1$ mm). Unlike the effects of k on g_a, the effects of leaf dimension (i.e., L) is equally sensed for all d_p. As the collection efficiency is larger for smaller particles (see Figure 5 and *Huang et al.* [2013, Figure S1-1]), this analysis further supports the argument that leaf dimension is the key contributor to the UFP collection when the depositing surfaces are considered as nearly smooth flat plates (i.e., $d_p < k \ll \delta$) as is the case here. Furthermore, the depositing

distance from the wall approximately equal to k when $d_p \ll k$ can be used to explain why the dependence of g_a on d_p gradually vanishes with increasing k (i.e., the lower boundary condition in equation (A9) is primarily dominated by k).

5. Conclusion

The UFP collection efficiency of four different broadleaf species under different wind speed conditions was characterized through wind tunnel measurements and interpreted through a porous media model. Despite the simplified representation of the turbulent transport process within the porous system, the model results and experiments deviate from each other by no more than 20% commensurate with measurement uncertainties. The modeled UFP collection term in the porous media approach was parameterized by two empirical parameters (γ and θ) as common to many UFP deposition approaches. The analysis here determined the optimum γ and θ for each species so as to match the measured penetration. The linkages between the optimum γ and θ and leaf attributes were explored using a standard three-sublayer deposition model for hydraulically smooth flat plates. The goal of this analysis was to generate expectations on how leaf dimension and microroughness impact γ and θ and subsequently UFP collection efficiency if analogies to hydraulically smooth flat plates are made. These expectations are then used to interpret patterns of optimum γ and θ inferred from the wind tunnel studies here across multiple species. Based on this analysis, the following can be concluded about the effects of microroughness and leaf dimension on γ and θ:

1. The value of γ generally increases with increasing k. However, γ can be treated as a constant ($\approx 2/3$) in the size range from 10 to 100 nm (i.e., UFP) when the leaf microroughness is $d_p < k \ll \delta$. For very small d_p (i.e., nucleation mode), particles tend to behave as gases with much larger γ values.
2. The value of θ increases with increasing k and increasing d_p suggesting that UFP collection efficiency can be enhanced by rougher surfaces even when k is in the hydraulically smooth regime (i.e., k remains immersed within the viscous sublayer). When the leaf dimension is reduced, resulting in a relatively smaller effective length scale for the quasi-laminar boundary layer to grow, θ increases. This θ increase with reduced leaf size leads to enhancements in the UFP collection efficiency for a given LAI. This finding is supported by the comparison of the optimized θ values from particle concentration measurements between four broadleaf species and one coniferous species in similar wind tunnel experiments at similar LAI. The UFP collection efficiency of Needleholly appears to be more efficient (i.e., larger θ) than the remaining three broadleaf species. Needleholly has less flexible texture and a geometric shape that shares some resemblance to conifers (especially at the leaf edge). That is, θ is sensitive to leaf geometry with higher values for cylindrically shaped foliage, lower values for flat-plate-like foliage, and intermediate values for foliage shapes that are partially flat plate but with edges that include cylindrical-like protrusions.

Current uncertainties in modeling the Brownian diffusion collection term can be reduced by future studies through experiments and theoretical model improvements, especially when leaf microroughness and along-wind effective leaf length scale are available. Furthermore, the findings here are only valid for a conceptual quasi-laminar boundary layer not protruded by microroughness elements. A survey of the literature suggests that $k < 1$ mm for numerous species as reported elsewhere [*Boize et al.*, 1976; *Burton and Bhushan*, 2006; *Hussein et al.*, 2013; *Kearns and Bärlocher*, 2008]. Given that $\delta \approx 1.2$ mm was also computed for typical field conditions hints that the latter assumption may not be too restrictive across many ecosystem types.

Appendix A: Particle Deposition Onto Hydraulically Smooth Plate

The three-sublayer depositional model, which has been implemented for smooth and rough surfaces across a wide range of particle sizes [*Browne*, 1974; *Davies*, 1966; *Hussein et al.*, 2012; *Lai and Nazaroff*, 2000; *Piskunov*, 2009; *Wood*, 1981; *Zhao and Wu*, 2006a, 2006b], is adopted. Only the UFP deposition onto hydraulically smooth flat plates is considered here. The theory for the three-sublayer depositional model is based on the relation between flux and concentration gradient given as

$$j = -(D_t + D_m)\frac{\partial C}{\partial y}, \tag{A1}$$

where j is the particle flux for a fixed particle diameter d_p and is assumed to be constant across the so-called particle concentration layer, which is contained within the quasi-laminar boundary adjacent to the plate surface, D_t is the particle turbulent diffusivity, D_m is the particle molecular diffusivity, C is the particle concentration, and y is the distance from the solid boundary. It is to be noted that the gravitational settling and the turbophoresis are negligible for UFP and are not considered here. Moreover, the particle turbulent diffusivity is usually assumed to be equal to the turbulent viscosity K_t for UFP [*Lin et al.*, 1953; *Lai and Nazaroff*, 2000; *Zhao and Wu*, 2006a]. This assumption is justified through the relation between D_t and K_t given as [*Hinze*, 1975]

$$D_t = K_t \left(1 + \frac{\tau_p}{\tau}\right)^{-1}, \tag{A2}$$

where τ_p and τ are the particle and turbulent relaxation time scales, respectively. For UFP, $\tau_p/\tau \ll 1$ resulting in $D_t \approx K_t$ [*Katul et al.*, 2010]. This assumption also implies that the interaction between UFP and the flow field is negligible. Stated differently, this assumption holds when the particles are small and sparsely distributed in the air medium [*Wood*, 1981]. Further accepting the assumption that the particle concentration far from the particle concentration layer C_∞ is constant (i.e., well-mixed conditions in air spaces most distant from foliage elements), the particle deposition velocity can be defined as

$$V_d = \frac{j}{C_\infty}. \tag{A3}$$

To normalize equation (A1) as common in smooth boundary layers, normalizations indicated by superscript + are based on the so-called wall units. All velocity normalizations are based on u_v. Thus, the dimensionless particle concentration, distance from the surface, and particle deposition velocity are respectively defined as

$$C^+ = \frac{C}{C_\infty}, \tag{A4}$$

$$y^+ = \frac{y u_v}{\nu}, \tag{A5}$$

$$V_d{}^+ = \frac{V_d}{u_v}, \tag{A6}$$

where u_v is the local friction velocity at the surface governed by the skin shear stress (i.e., viscous drag c_v) and ν is the air kinematic viscosity. By substituting the dimensionless variables into equation (A1), the normalized form of equation (A1) can be written as

$$V_d{}^+ = \left(\frac{K_t + D_m}{\nu}\right)\frac{\partial C^+}{\partial y^+}. \tag{A7}$$

To solve equation (A7), the turbulent viscosity as a function of y^+, which can be obtained from either measurements or direct numerical simulation as summarized elsewhere [*Hussein et al.*, 2012], is required. Fitting a power law expression to the results of direct numerical simulation reported elsewhere [*Kim et al.*, 1987] yields [*Lai and Nazaroff*, 2000; *Piskunov*, 2009]

$$\frac{K_t}{\nu} = \begin{cases} 7.669 \times 10^{-4}(y^+)^3; & 0 \le y^+ \le 4.3 \\ 10^{-3}(y^+)^{2.8214}; & 4.3 \le y^+ \le 12.5 \\ 1.07 \times 10^{-2}(y^+)^{1.8895}; & 12.5 \le y^+ \le 30 \end{cases}. \tag{A8}$$

For a hydraulically smooth surface, the effective height of roughness element k must be smaller than the thickness of the quasi-laminar boundary (i.e., the dimensionless roughness height $k^+ = ku_v/\nu \le 4.3$). For such a smooth surface, the microroughness elements do not alter the flow field given by equation (A8)

though they can alter particle deposition. Since j is constant, ${V_d}^+$ is also constant under certain u_v conditions. Integration of equation (A7) with boundary conditions set as $C^+ = 0$ at $y^+ = y_0^+$ and $C^+ = 1$ at $y^+ = 30$ (i.e., $C = C_\infty$ outside the outer edge of the buffer layer) yields

$$\frac{1}{{V_d}^+} = \int_{y_0^+}^{30} \frac{1}{\left(\frac{K_t}{\nu} + \frac{D_m}{\nu}\right)} \mathrm{d}y^+, \tag{A9}$$

$${y_0}^+ = \frac{u_v}{\nu}\left(\frac{d_p}{2} + k\right) = r^+ + k^+,$$

where r^+ (= $d_p u_v / 2\nu$) is the dimensionless particle radius. It should be noted that the velocity profile is not displaced here for hydraulically smooth surfaces but the effect of the roughness element is included assuming the plate surface is a perfect sink. Thus, the integral in equation (A9) can be expressed as

$$\frac{1}{{V_d}^+} = I(r^+, k^+) = M(r^+, k^+){S_c}^{2/3} + N(r^+), \tag{A10}$$

where $S_c = \nu / D_m$ is, as before, the particle Schmidt number. On the right-hand side, the first term is the integration of equation (A9) across the quasi-laminar boundary (i.e., ${y_0}^+ \le y^+ \le 4.3$) and $M(r^+, k^+)$ is a parameter that varies with the dimensionless particle radius r^+ and the dimensionless roughness height k^+. The analytical solution for $M(r^+, k^+)$ has been derived elsewhere [*Lai and Nazaroff*, 2000] and can be expressed as

$$M(r^+, k^+) = 3.64(a - b),$$

$$a = \sqrt{3}\tan^{-1}\left(\frac{2 \times 4.3 - 10.92{S_c}^{-1/3}}{10.92\sqrt{s}{S_c}^{-1/3}}\right) + \frac{1}{2}\left[\frac{\left({S_c}^{-1/3} + \frac{4.3}{10.92}\right)^3}{{S_c}^{-1} + \left(\frac{4.3}{10.92}\right)^3}\right], \tag{A11}$$

$$b = \sqrt{3}\tan^{-1}\left(\frac{2 \times {y_0}^+ - 10.92{S_c}^{-1/3}}{10.92\sqrt{s}{S_c}^{-1/3}}\right) + \frac{1}{2}\left[\frac{\left({S_c}^{-1/3} + \frac{{y_0}^+}{10.92}\right)^3}{{S_c}^{-1} + \left(\frac{{y_0}^+}{10.92}\right)^3}\right].$$

The second term, $N(r^+)$, is the integration of equation (A9) across the buffer layer (i.e., $4.3 \le y^+ \le 30$) and is only associated with r^+. The differences between the formulation here and that of *Lai and Nazaroff* [2000] is that the effect of roughness elements for hydraulically smooth surface and D_m outside the quasi-laminar boundary layer are excluded in *Lai and Nazaroff* [2000] but included here. For convenience, equation (A10) can be simply written as

$$j = \frac{u_v}{I(r^+, k^+)} C_\infty = g_a C_\infty, \tag{A12}$$

$$g_a = u_v (M(r^+, k^+){S_c}^{2/3} + N(r^+))^{-1},$$

where g_a is the particle boundary layer conductance assuming that Brownian diffusion dominates the UFP collection mechanism. To compute V_d, two parameters must be a priori specified for predicting g_a: k and u_v as governed by the skin friction (i.e., viscous drag).

Appendix B: Bridging the Quasi-Laminar Boundary Layer Conductance to the Three-Sublayer Depositional Model

Upon equating g_a from equation (4) for the vegetated medium and equation (A12) for such a hydraulically smooth but finite plate, the dimensionless conductance $g_{a_*} = g_a / u_\tau$ spatially averaged over L can be

expressed as

$$g_{a_*} = \theta S_c^{-\gamma} = \left(\frac{u_v}{u_\tau}\right)\left(M(r^+,k^+)S_c^{2/3} + N(r^+)\right)^{-1}. \quad \text{(B1)}$$

By retaining the same form of g_a as equation (4) and adopting the velocity-squared law (i.e., $u_v^2 = c_v U^2$ and $u_\tau^2 = C_d U^2$) to describe the local momentum transfer [*Monteith and Unsworth*, 1990; *Taylor*, 1916; *Thom*, 1968; *Yi*, 2008], equation (B1) can be further simplified to yield

$$g_{a_*} = \left[\left(\frac{c_v}{C_d}\right)^{1/2} M(r^+,k^+)^{-1}\right] S_c^{-\gamma},$$

$$\theta = \left(\frac{c_v}{C_d}\right)^{1/2} M(r^+,k^+)^{-1}, \quad \text{(B2)}$$

$$\gamma = \frac{\log\left(S_c^{2/3} + \frac{N(r^+)}{M(r^+,k^+)}\right)}{\log(S_c)},$$

where γ is expressed as a function of d_p as well as k, and θ is connected to k through $M(r^+,k^+)^{-1}$ and $(c_v/C_d)^{1/2}$ that is linked to leaf dimension (see discussions in section 4.3). Thus, an index I_1 can now be employed to explore the effects of k on θ, given as

$$I_1(r^+,k^+) = \theta \Big/ \left(\frac{c_v}{C_d}\right)^{1/2} = M(r^+,k^+)^{-1}. \quad \text{(B3)}$$

Otherwise, another index I_2 can be defined as

$$I_2 = \theta M(r^+,k^+) = \left(\frac{c_v}{C_d}\right)^{1/2}, \quad \text{(B4)}$$

which is used to explore how leaf dimension impacts θ through $(c_v/C_d)^{1/2}$ for a given microroughness and flow conditions. Moreover, another dimensionless conductance g_k given by

$$g_k = M(r^+,k^+)^{-1} S_c^{-\gamma} \quad \text{(B5)}$$

can further assist the analysis for compensatory effects of k and leaf dimension on θ (see discussions in section 4.3.4)

Acknowledgments

G.G. Katul and C.W. Huang acknowledge support from the National Science Foundation (NSF-AGS-1102227 and NSF-EAR-134470), the United States Department of Agriculture (2011-67003-30222), and the U.S. Department of Energy (DOE) through the office of Biological and Environmental Research (BER) Terrestrial Ecosystem Science (TES) Program (DE-SC0006967 and DE-SC0011461). M.Y. Lin acknowledges Taiwan's Ministry of Science and Technology (MOST 102-2218-E-006-002-MY2 and 103-2622-E-006-018-CC2) and the Headquarters of University Advancement at the National Cheng Kung University for their support. The experimental data used in this paper are available upon request from any of the authors through e-mail (Huang: cheng.wei.huang@duke.edu, Lin: m_lin@mail.ncku.edu.tw, Khlystov: andrey.khlystov@dri.edu, and Katul: gaby@duke.edu).

References

Altshuller, A. (1985), Relationships involving fine particle mass, fine particle sulfur and ozone during episodic periods at sites in and around St. Louis, MO, *Atmos. Environ.*, *19*(2), 265–276.

Andreae, M. O., and P. J. Crutzen (1997), Atmospheric aerosols: Biogeochemical sources and role in atmospheric chemistry, *Science*, *276*(5315), 1052–1058.

Beckett, K. P., P. H. Freer-Smith, and G. Taylor (2000), Particulate pollution capture by urban trees: Effect of species and windspeed, *Global Change Biol.*, *6*(8), 995–1003.

Boize, L., C. Gudin, and G. Purdue (1976), The influence of leaf surface roughness on the spreading of oil spray drops, *Ann. Appl. Biol.*, *84*(2), 205–211.

Browne, L. W. B. (1974), Deposition of particles on rough surfaces during turbulent gas-flow in a pipe, *Atmos. Environ.*, *8*(8), 801–816.

Brunet, Y., J. J. Finnigan, and M. R. Raupach (1994), A wind tunnel study of air flow in waving wheat: Single-point velocity statistics, *Boundary Layer Meteorol.*, *70*(1-2), 95–132.

Buckley, A. J., M. D. Wright, and D. L. Henshaw (2008), A technique for rapid estimation of the charge distribution of submicron aerosols under atmospheric conditions, *Aerosol Sci. Technol.*, *42*(12), 1042–1051.

Burton, Z., and B. Bhushan (2006), Surface characterization and adhesion and friction properties of hydrophobic leaf surfaces, *Ultramicroscopy*, *106*(8), 709–719.

Buzea, C., I. I. Pacheco, and K. Robbie (2007), Nanomaterials and nanoparticles: Sources and toxicity, *Biointerphases*, *2*(4), MR17–MR71.

Cao, J. X., Y. Tamura, and A. Yoshida (2012), Wind tunnel study on aerodynamic characteristics of shrubby specimens of three tree species, *Urban For. Urban Greening*, *11*(4), 465–476.

Davidson, C. I., J. M. Miller, and M. A. Pleskow (1982), The influence of surface-structure on predicted particle dry deposition to natural grass canopies, *Water Air Soil Pollut.*, *18*(1-3), 25–43.

Davies, C. N. (1966), *Aerosol Science*, vol. 1102, Academic Press, London.

Feng, J. (2008), A size-resolved model and a four-mode parameterization of dry deposition of atmospheric aerosols, *J. Geophys. Res.*, *113*, D12201, doi:10.1029/2007JD009004.
Finnigan, J. (2000), Turbulence in plant canopies, *Annu. Rev. Fluid Mech.*, *32*, 519–571.
Finnigan, J. J., and S. E. Belcher (2004), Flow over a hill covered with a plant canopy, *Q. J. R. Meteorol. Soc.*, *130*(596), 1–29.
Freer-Smith, P. H., A. A. El-Khatib, and G. Taylor (2004), Capture of particulate pollution by trees: A comparison of species typical of semi-arid areas (*Ficus nitida* and *Eucalyptus globulus*) with European and North American species, *Water Air Soil Pollut.*, *155*(1-4), 173–187.
Hinze, J. O. (1975), *Turbulence*, McGraw-Hill, New York.
Holmn, B. A., and A. Ayala (2002), Ultrafine PM emissions from natural gas, oxidation-catalyst diesel, and particle-trap diesel heavy-duty transit buses, *Environ. Sci. Technol.*, *36*(23), 5041–5050.
Huang, C. W., M. Y. Lin, A. Khlystov, and G. G. Katul (2013), The effects of leaf area density variation on the particle collection efficiency in the size range of ultrafine particles (UFP), *Environ. Sci. Technol.*, *47*(1), 11,607–11,615.
Huang, C. W., S. Launiainen, T. Grönholm, and G. G. Katul (2014), Particle deposition to forests: An alternative to K-theory, *Atmos. Environ.*, *94*, 593–605.
Hussein, T., J. Smolik, V. M. Kerminen, and M. Kulmala (2012), Modeling dry deposition of aerosol particles onto rough surfaces, *Aerosol Sci. Technol.*, *46*(1), 44–59.
Hussein, T., V. Norros, J. Hakala, T. Petj, P. P. Aalto, I. Rannik, T. Vesala, and O. Ovaskainen (2013), Species traits and inertial deposition of fungal spores, *J. Aerosol Sci.*, *61*, 81–98.
Hwang, H. J., S. J. Yook, and K. H. Ahn (2011), Experimental investigation of submicron and ultrafine soot particle removal by tree leaves, *Atmos. Environ.*, *45*(38), 6987–6994.
Katul, G. G., T. Grönholm, S. Launiainen, and T. Vesala (2010), Predicting the dry deposition of aerosol-sized particles using layer-resolved canopy and pipe flow analogy models: Role of turbophoresis, *J. Geophys. Res.*, *115*, D12202, doi:10.1029/2009JD012853.
Katul, G. G., T. Grönholm, S. Launiainen, and T. Vesala (2011), The effects of the canopy medium on dry deposition velocities of aerosol particles in the canopy layer above forested ecosystems, *Atmos. Environ.*, *45*(5), 1203–1212.
Kearns, S. G., and F. Bärlocher (2008), Leaf surface roughness influences colonization success of aquatic hyphomycete conidia, *Fungal Ecol.*, *1*(1), 13–18.
Kim, J., P. Moin, and R. Moser (1987), Turbulence statistics in fully developed channel flow at low Reynolds number, *J. Fluid Mech.*, *177*, 133–166.
Lai, A. C. K., and W. W. Nazaroff (2000), Modeling indoor particle deposition from turbulent flow onto smooth surfaces, *J. Aerosol Sci.*, *31*(4), 463–476.
Lin, C. S., R. W. Moulton, and G. L. Putnam (1953), Mass transfer between solid wall and fluid streams. Mechanism and eddy distribution relationships in turbulent flow, *Ind. Eng. Chem.*, *45*(3), 636–640.
Lin, M. Y., and A. Khlystov (2012), Investigation of ultrafine particle deposition to vegetation branches in a wind tunnel, *Aerosol Sci. Technol.*, *46*(4), 465–472.
Lin, M. Y., G. G. Katul, and A. Khlystov (2012), A branch scale analytical model for predicting the vegetation collection efficiency of ultrafine particles, *Atmos. Environ.*, *51*, 293–302.
Lin, M. Y., A. Khlystov, and G. G. Katul (2014), Vegetation collection efficiency of ultrafine particles: From single fiber to porous media, *J. Geophys. Res. Atmos.*, *119*, 222–229, doi:10.1002/2013JD020917.
McMurry, P. H., and J. C. Wilson (1982), Growth laws for the formation of secondary ambient aerosols—Implications for chemical conversion mechanisms, *Atmos. Environ.*, *16*(1), 121–134.
Molina-Aiz, F. D., D. L. Valera, A. J. Alvarez, and A. Madueno (2006), A wind tunnel study of airflow through horticultural crops: Determination of the drag coefficient, *Biosystems Eng.*, *93*(4), 447–457.
Monteith, J. L., and M. H. Unsworth (1990), *Principles of Environmental Physics*, Edward Arnold, New York.
Oberdörster, G. (2001), Pulmonary effects of inhaled ultrafine particles, *Int. Arch. Occup. Environ. Health*, *74*(1), 1–8.
Oberdörster, G., E. Oberdörster, and J. Oberdörster (2005), Nanotoxicology: An emerging discipline evolving from studies of ultrafine particles, *Environ. Health Perspect.*, *113*(7), 823–839.
Peters, A., H. E. Wichmann, T. Tuch, J. Heinrich, and J. Heyder (1997), Respiratory effects are associated with the number of ultrafine particles, *Am. J. Respir. Crit. Care Med.*, *155*(4), 1376–1383.
Petroff, A., A. Mailliat, M. Amielh, and F. Anselmet (2008a), Aerosol dry deposition on vegetative canopies. Part I: Review of present knowledge, *Atmos. Environ.*, *42*(16), 3625–3653.
Petroff, A., A. Mailliat, M. Amielh, and F. Anselmet (2008b), Aerosol dry deposition on vegetative canopies. Part II: A new modelling approach and applications, *Atmos. Environ.*, *42*(16), 3654–3683.
Piskunov, V. N. (2009), Parameterization of aerosol dry deposition velocities onto smooth and rough surfaces, *J. Aerosol Sci.*, *40*(8), 664–679.
Poggi, D., A. Porporato, L. Ridolfi, J. D. Albertson, and G. G. Katul (2004), The effect of vegetation density on canopy sub-layer turbulence, *Boundary Layer Meteorol.*, *111*(3), 565–587.
Prandtl, L. (1925), A report on testing for built-up turbulence, *Z. Angew. Math. Mech.*, *5*, 136–139.
Pryor, S. C., R. J. Barthelmie, L. L. Sørensen, S. E. Larsen, A. M. Sempreviva, T. Grönholm, Ü. Rannik, M. Kulmala, and T. Vesala (2008a), Upward fluxes of particles over forests: When, where, why?, *Tellus Ser. B*, *60*(3), 372–380, doi:10.1111/j.1600-0889.2008.00341.x.
Pryor, S. C., et al. (2008b), A review of measurement and modelling results of particle atmosphere-surface exchange, *Tellus Ser. B*, *60*(1), 42–75.
Pryor, S. C., R. J. Barthelmie, A. M. Spaulding, S. E. Larsen, and A. Petroff (2009), Size-resolved fluxes of sub-100-nm particles over forests, *J. Geophys. Res.*, *114*, D18212, doi:10.1029/2009JD012248.
Raupach, M. R. (1994), Simplified expressions for vegetation roughness length and zero-plane displacement as functions of canopy height and area index, *Boundary Layer Meteorol.*, *71*(1-2), 211–216.
Raupach, M. R., and A. S. Thom (1981), Turbulence in and above plant canopies, *Annu. Rev. Fluid Mech.*, *13*, 97–129.
Schlichting, H. (1979), *Boundary-Layer Theory*, McGraw-Hill, New York.
Seinfeld, J. H., and S. N. Pandis (2006), *Atmospheric Chemistry and Physics: From Air Pollution to Climate Change*, John Wiley, N. J.
Sexton, J. O., X. P. Song, M. Feng, P. Noojipady, A. Anand, C. Q. Huang, D. H. Kim, K. M. Collins, S. Channan, and C. DiMiceli (2013), Global, 30-m resolution continuous fields of tree cover: Landsat-based rescaling of MODIS vegetation continuous fields with lidar-based estimates of error, *Int. J. Digital Earth*, *6*(5), 427–448.
Slinn, W. G. N. (1982), Predictions for particle deposition to vegetative canopies, *Atmos. Environ.*, *16*(7), 1785–1794.

Stoy, P. C., G. G. Katul, M. Siqueira, J.-Y. Juang, K. A. Novick, J. M. Uebelherr, and R. Oren (2006), An evaluation of models for partitioning eddy covariance-measured net ecosystem exchange into photosynthesis and respiration, *Agric. For. Meteorol.*, *141*(1), 2–18.

Taylor, G. I. (1916), Skin friction of the wind on the Earth's surface, *Proc. R. Soc. London, Ser. A*, *92*(637), 196–199.

Thom, A. S. (1968), Exchange of momentum, mass, and heat between an artificial leaf and airflow in a wind-tunnel, *Q. J. R. Meteorol. Soc.*, *94*(399), 44–55.

Wesely, M. L., and B. B. Hicks (2000), A review of the current status of knowledge on dry deposition, *Atmos. Environ.*, *34*(12-14), 2261–2282.

Wood, N. B. (1981), A simple method for the calculation of turbulent deposition to smooth and rough surfaces, *J. Aerosol Sci.*, *12*(3), 275–290.

Yi, C. X. (2008), Momentum transfer within canopies, *J. Appl. Meteorol. Climatol.*, *47*(1), 262–275.

Zhang, L. M., S. L. Gong, J. Padro, and L. Barrie (2001), A size-segregated particle dry deposition scheme for an atmospheric aerosol module, *Atmos. Environ.*, *35*(3), 549–560.

Zhao, B., and J. Wu (2006a), Modeling particle deposition from fully developed turbulent flow in ventilation duct, *Atmos. Environ.*, *40*(3), 457–466.

Zhao, B., and J. Wu (2006b), Modeling particle deposition onto rough walls in ventilation duct, *Atmos. Environ.*, *40*(36), 6918–6927.

Zimmerman, P., R. Chatfield, J. Fishman, P. Crutzen, and P. Hanst (1978), Estimates on the production of CO and H_2 from the oxidation of hydrocarbon emissions from vegetation, *Geophys. Res. Lett.*, *5*(8), 679–682.